The Astrophysical Journal, 620:961–969, 2005 February 20


# DIAMETERS OF MIRA STARS MEASURED SIMULTANEOUSLY IN THE *J*, *H*, AND *K′* NEAR-INFRARED BANDS

R. Millan-Gabet,[1] E. Pedretti,[2,3] J. D. Monnier,[2] F. P. Schloerb,[4] W. A. Traub,[5] N. P. Carleton,[5] M. G. Lacasse,[5] and D. Segransan[6]

*Received 2004 September 2; accepted 2004 October 21*

## ABSTRACT

We present the first spatially resolved observations of a sample of 23 Mira stars simultaneously measured in the near-infrared *J*, *H*, and *K′* bands. The technique used was optical long-baseline interferometry, and we present for each star visibility amplitude measurements as a function of wavelength. We also present characteristic sizes at each spectral band, obtained by fitting the measured visibilities to a simple uniform disk model. This approach reveals the general relation *J* diameter < *H* diameter < *K′* diameter.

*Subject headings:* instrumentation: interferometers — stars: atmospheres — stars: fundamental parameters — stars: variables: other — techniques: high angular resolution

*Online material:* machine-readable table

## 1. INTRODUCTION

Mira stars are variable, pulsating stars in the asymptotic giant branch. They have pulsation periods of about 100–1000 days, during which their light curves exhibit large amplitude variations (as high as 10 mag at visual wavelengths, becoming a more modest ∼1 mag in the near-infrared) and their spectral types vary by a few subclasses. During the pulsation cycle, their photospheric radii are thought to vary by 5%–50%. Mira star atmospheres are geometrically extended and have very low effective temperatures (≲3000 K); hence, they have a rich molecular composition. They exhibit high mass-loss rates (a few times $10^{-6}\,M_{\odot}\,\mathrm{yr}^{-1}$), and the ejected material forms layers that become sites of circumstellar maser activity and dust formation. Thus, although the Mira evolutionary stage is relatively short ($\sim 5 \times 10^5$ yr), it is a crucial one in order to understand a variety of phenomena such as high mass loss, the formation of planetary nebulae, and the chemical enrichment of the galaxy.

Despite the existing large body of observational and theoretical work, many aspects of the physics of Mira stars remain poorly understood, in particular, their detailed atmospheric stratification and composition and their dominant mode of pulsation. This is, to a large extent, a consequence of their intrinsic complexity (treatment of three-dimensional convection, photospheric shocks, and rich photospheric chemistry), and new observational data that can help discriminate between the large number of theoretical models that have been proposed are most needed.

Spatially resolved observations of Mira stars are clearly desirable and can be easily obtained using high-resolution techniques such as long-baseline interferometry. The geometrically extended and chemically rich nature of Mira star atmospheres manifests itself in apparent physical sizes that depend on the wavelength of observation, especially when crossing regions in the spectrum in which the opacity changes rapidly. This fact was first observed in the visible region of the spectrum, where sizes as much as 50% smaller are found in narrowband near-continuum filters than in filters contaminated by TiO absorption (Bonneau & Labeyrie 1973; Labeyrie et al. 1977; Bonneau et al. 1982; Haniff et al. 1995; Hofmann et al. 2000, 2001).

Although originally expected to be better probes of the underlying stellar continuum, measurements at infrared wavelengths also exhibit nontrivial wavelength dependence. Synthesizing measurements obtained at different facilities, it appears that as a general trend Mira sizes appear large in the visible (Tuthill et al. 1994; Haniff et al. 1995; Ireland et al. 2004b), smaller in the near-infrared (Perrin et al. 1999; Hofmann et al. 2002; van Belle et al. 2002, and references therein), and larger again at thermal infrared wavelengths (Mennesson et al. 2002; Weiner et al. 2003a, 2003b). The interpretation of this broad trend is that the outer layers (i.e., those layers above a level that could be called "the photosphere") are relatively obscuring in the visible, relatively transparent in the near-infrared, and again relatively obscuring in the thermal infrared band. The physical basis for this variation of opacity with wavelength can be modeled once the underlying empirical variation of diameters with wavelength is established by observations. The purpose of this paper is to show that there is such a variation through the near-infrared, as defined by the *J*, *H*, and *K′* bands.

Because of instrumental limitations, *simultaneous* measurements at different wavelengths are scarce in the literature, but they are clearly the optimum way to explore the wavelength-dependent structure, since Mira stars are suspected of exhibiting important cycle-to-cycle nonrepeatability. Dramatic size increases (25%–100%) have been observed between near- (∼1.1–2.3 μm) and thermal (∼3.1–3.8 μm) infrared measurements, both in narrow (Tuthill et al. 2000a, 2000b) and broad bands (Mennesson et al. 2002). Smaller but significant (1%–20%) effects have been observed in narrow bands within the near-infrared *K* band (∼2.0–2.4 μm), as the narrow filters preferentially sample portions of the spectrum corresponding to strong molecular bands or the adjacent continuum (Thompson 2002; Thompson et al. 2002; Perrin et al. 2004). Using the same portion of the spectrum as in this work, Weigelt et al. (2003) studied the visibility of the Mira star T Cep dispersed across the *J*, *H*, and *K* bands, finding

[1] Michelson Science Center, California Institute of Technology, MS 100-22, Pasadena, CA 91125; rafael@ipac.caltech.edu.
[2] Astronomy Department, University of Michigan, 501 East University Avenue, Ann Arbor, MI 48109.
[3] NASA Michelson postdoctoral fellow.
[4] Astronomy Department, University of Massachusetts at Amherst, 710 North Pleasant Street, Amherst, MA 01003.
[5] Harvard-Smithsonian Center for Astrophysics, 60 Garden Street, Cambridge, MA 02138.
[6] Observatoire de Genève, Chemin des Maillettes 51, CH-1290 Sauverny, Switzerland.

TABLE 1
Basic Properties of Mira Star Sample

| Name | R.A. (J2000.0) | Decl. (J2000.0) | $V_{min} - V_{max}$ | $J$ | $H$ | $K$ | Spectral Type | Distance | Distance Reference |
|---|---|---|---|---|---|---|---|---|---|
| R And..... | 00 24 01.95 | +38 34 37.3 | 7 − 15 | 2.0 | 0.7 | 0.1 | S | 532 ± 101 | 1 |
| Z Cet..... | 01 06 45.13 | −01 28 52.9 | 9 − 14 | 4.6 | 3.7 | 3.3 | M5 | 920 ± 175 | 2 |
| U Per..... | 01 59 35.12 | +54 49 20.0 | 8 − 12 | 2.2 | 1.2 | 0.9 | M6 | 559 ± 140 | 3 |
| R Per..... | 03 30 02.98 | +35 40 17.1 | 9 − 14 | 4.8 | 4.0 | 3.2 | M4 | ... | ... |
| R Aur..... | 05 17 17.69 | +53 35 10.0 | 7 − 13 | 1.0 | −0.1 | −0.5 | M7 | 342 ± 85 | 3 |
| S Ori..... | 05 29 00.89 | −04 41 32.7 | 8 − 14 | 0.9 | −0.01 | −0.5 | M7 | 481 ± 120 | 3 |
| U Ori..... | 05 55 49.17 | +20 10 30.7 | 6 − 13 | 1.1 | 0.2 | −0.3 | M8 | 310 ± 77 | 3 |
| X Aur..... | 06 12 13.38 | +50 13 40.4 | 8 − 14 | 4.5 | 3.8 | 3.2 | K2 | ... | ... |
| R Cnc..... | 08 16 33.83 | +11 43 34.5 | 6 − 11 | 0.8 | −0.3 | −0.7 | M7 | 300 ± 30 | 4 |
| R LMi..... | 09 45 34.28 | +34 30 42.8 | 8 − 13 | 1.7 | 0.5 | −0.1 | M7 | 367 ± 22 | 3 |
| R Leo..... | 09 47 33.49 | +11 25 43.6 | 6 − 10 | −0.7 | −1.7 | −2.3 | M8 | 115 ± 29 | 3 |
| R Hya..... | 13 29 42.78 | −23 16 52.8 | 5 − 8 | −1.3 | −2.2 | −2.7 | M7 | 110 ± 21 | 2 |
| W Hya..... | 13 49 02.00 | −28 22 03.5 | 6 − 9 | −1.7 | −2.6 | −3.2 | M7 | 80 ± 15 | 2 |
| S Crb..... | 15 21 23.96 | +31 22 02.6 | 7 − 13 | 1.1 | 0.2 | −0.2 | M7 | 375 ± 94 | 3 |
| RS Lib..... | 15 24 19.79 | −22 54 39.9 | 7 − 13 | 1.0 | −0.1 | −0.6 | M | 210 ± 40 | 5 |
| R Ser..... | 15 50 41.73 | +15 08 01.1 | 6 − 14 | 1.3 | 0.4 | 0.1 | M7 | 356 ± 89 | 3 |
| S Her..... | 16 51 53.92 | +14 56 30.8 | 6 − 13 | 2.3 | 1.2 | 1.0 | M6 | 677 ± 169 | 3 |
| Ry Lyr..... | 18 44 51.90 | +34 40 30.0 | 10 − 15 | ... | ... | ... | M6 | ... | ... |
| R Aql..... | 19 06 22.20 | +08 13 48.0 | 6 − 12 | 0.7 | −0.3 | −0.8 | M7 | 224 ± 56 | 3 |
| R Peg..... | 23 06 39.20 | +10 32 36.1 | 7 − 13 | 1.8 | 0.9 | 0.4 | M7 | 435 ± 109 | 3 |
| W Peg..... | 23 19 50.50 | +26 16 43.7 | 8 − 13 | 1.1 | 0.2 | −0.1 | M7 | 310 ± 31 | 4 |
| S Peg..... | 23 20 32.60 | +08 55 08.1 | 8 − 13 | 2.3 | 1.4 | 1.0 | M6 | 675 ± 169 | 3 |
| R Aqr..... | 23 43 49.50 | −15 17 04.2 | 6.5 − 11 | −0.1 | −1.1 | −1.6 | M7 | 272 ± 68 | 3 |

Notes.—Units of right ascension are hours, minutes, and seconds, and units of declination are degrees, arcminutes, and arcseconds. $V$ magnitudes and spectral types are from the AAVSO and SIMBAD databases, and near-infrared magnitudes are from the 2MASS database. As these stars are by definition variable, this information is meant to be merely representative.

References.—(1) Van Belle et al. 1997; (2) Jura & Kleinmann 1992; (3) van Belle et al. 2002; (4) Wyatt & Cahn 1983; (5) Young 1995.

similar $J$ and $H$ sizes that are ~10% smaller than the $K$-band size as well as size differences within the $K$ band as large as 26%.

Clearly, the richness of the size-wavelength relation holds the potential to be the best probe of atmospheric structure in these stars. In turn, as has been illustrated in the recent multiwavelength modeling effort by Perrin et al. (2004), a complete model that includes the stellar photosphere, dominant opacity sources, and possible additional emitting layers must be globally fitted in order to also extract accurate stellar diameters and derive conclusions about the pulsation mode.

In this paper we present the first systematic survey of Mira star diameters measured near simultaneously in the near-infrared $J$, $H$, and $K'$ bands. This new multicolor data set allows us in particular to derive apparent size ratios, which are immune to many sources of calibration error. In § 2 we describe the measurement technique and Mira sample observed, and in § 3 we describe the data analysis procedure. In § 4 we present our results, both in the form of uniform diameter fits at each spectral band in order to illustrate the main trends in these wavelength regions and as tables of calibrated visibility data for straightforward use in global fitting including other data sets. In § 5 we discuss our main results and place them in the context of recent theoretical work.

## 2. OBSERVATIONS

Observations were carried out at the Infrared Optical Telescope Array (IOTA), a long-baseline interferometer located on Mount Hopkins, AZ (see, e.g., Traub 1998). The data presented here were obtained using the two telescopes available at the time on two configurations that provide physical baseline lengths of approximately 21 and 38 m at geographic azimuth angles (measured east of north) of $-4^\circ$ and $+18^\circ$, respectively.

The beam combination and fringe detection instrumentation is exactly as described in Millan-Gabet (1999) and Millan-Gabet et al. (2001). In short, afocal telescope beams were combined at a bulk optics beam combiner, and interferograms were produced by modulating the optical path difference (OPD) between the two beams by $\pm 60$ $\mu$m. The fringe modulation frequencies are in the range 100–2000 Hz, chosen as an optimum trade-off between maximizing the photon signal and minimizing the readout time to freeze out atmospherically induced OPD variations during the fringe acquisition. The two outputs of the beam splitter were focused on two well-separated pixels of a NICMOS3 array, the readout of which is synchronized with the optical path modulation (Millan-Gabet et al. 1999).

The NICMOS3 camera contains a set of three standard near-infrared $J$ ($\lambda_0 = 1.25$ $\mu$m, $\Delta\lambda = 0.28$ $\mu$m), $H$ ($\lambda_0 = 1.65$ $\mu$m, $\Delta\lambda = 0.30$ $\mu$m) and $K'$ ($\lambda_0 = 2.16$ $\mu$m, $\Delta\lambda = 0.32$ $\mu$m) filters, where $\lambda_0$ and $\Delta\lambda$ are the center wavelength and full width at half-maximum, respectively. Rapid switching between the three filters guaranteed near-simultaneous observations (within a few minutes) in the three bands.

A typical observation consisted of 500 interferograms, obtained in a few minutes, followed by a measurement of the sky background. Target observations are interleaved with an identical sequence obtained on calibrator stars that are unresolved by the interferometer or have small diameters that can be estimated. This sequence was repeated for each of the three filters.

The basic properties of the Mira stars observed are listed in Table 1, and a log of observations is given in Table 2.

## 3. DATA ANALYSIS AND VALIDATION

The data reduction and calibration procedures are also essentially the same as those described in Millan-Gabet (1999)

TABLE 2
Log of Observations

| Name | Date | Julian Date (−2,450,000) | Baseline | Filters | Calibrator(s) |
|---|---|---|---|---|---|
| R And | 1997 Nov 21 | 774.0 | S15N35 | $H/K'$ | HR 82, HR 175 |
| Z Cet | 1998 Nov 4 | 1122.0 | S15N35 | $J/H/K'$ | HR 353 |
| U Per | 1997 Nov 19 | 772.0 | S15N35 | $J/H/K'$ | HR 787 |
| U Per | 1998 Oct 1 | 1088.0 | S15N35 | $J/H/K'$ | HR 470 |
| R Per | 1998 Oct 2 | 1089.0 | S15N35 | $J/H/K'$ | HR 876 |
| R Per | 1998 Nov 5 | 1123.0 | S15N35 | $J/H/K'$ | HR 876 |
| R Aur | 1997 Oct 12 | 734.0 | S15N15 | $J/H$ | HR 1866 |
| R Aur | 1997 Nov 19 | 772.0 | S15N35 | $H/K'$ | HR 1588, HR 1866 |
| R Aur | 1997 Nov 22 | 775.0 | S15N35 | $H/K'$ | HR 1588 |
| S Ori | 1998 Nov 5 | 1123.0 | S15N35 | $H/K'$ | HR 1830 |
| U Ori | 1997 Oct 17 | 739.0 | S15N15 | $J/H$ | HR 2169 |
| U Ori | 1997 Nov 21 | 774.0 | S15N35 | $K'$ | HR 2047 |
| U Ori | 1997 Nov 23 | 776.0 | S15N35 | $H/K'$ | HR 2047 |
| X Aur | 1997 Oct 14 | 736.0 | S15N15 | $J/H/K'$ | HR 2338 |
| R Cnc | 1998 Mar 2 | 875.0 | S15N15 | $H/K'$ | HR 2864 |
| R LMi | 1997 Nov 20 | 773.0 | S15N35 | $K'$ | HR 3791 |
| R LMi | 1998 Feb 28 | 873.0 | S15N15 | $J/H/K'$ | HR 4081 |
| R LMi | 1998 Mar 2 | 875.0 | S15N15 | $J/H/K'$ | HR 4081 |
| R Leo | 1998 Mar 1 | 874.0 | S15N15 | $H/K'$ | HR 3877 |
| R Hya | 1998 Feb 28 | 873.0 | S15N15 | $J/H/K'$ | HR 5020, HR 4958 |
| R Hya | 1998 Mar 2 | 875.0 | S15N15 | $J/H/K'$ | HR 5020, HR 4958 |
| W Hya | 1998 Mar 1 | 874.0 | S15N15 | $H/K'$ | HR 5312 |
| S Crb | 1998 Mar 1 | 874.0 | S15N15 | $J/H/K'$ | HR 5674 |
| S Crb | 1998 Jun 12 | 977.0 | S15N35 | $H/K'$ | HR 5674 |
| RS Lib | 1998 Feb 28 | 873.0 | S15N15 | $J/H/K'$ | HR 5824 |
| R Ser | 1998 Mar 2 | 875.0 | S15N15 | $J/H/K'$ | HR 5940 |
| R Ser | 1998 Mar 7 | 880.0 | S15N35 | $H/K'$ | HR 5940 |
| S Her | 1998 Jun 15 | 980.0 | S15N35 | $J/H$ | HR 6542, HR 6065 |
| Ry Lyr | 1998 Jun 15 | 980.0 | S15N35 | $H/K'$ | HR 7192 |
| R Aql | 1998 Jun 13 | 978.0 | S15N35 | $H/K'$ | HR 7557 |
| R Peg | 1998 Oct 1 | 1088.0 | S15N35 | $J/H/K'$ | HR 8608 |
| W Peg | 1998 Oct 1 | 1088.0 | S15N35 | $H/K'$ | HR 9051 |
| S Peg | 1998 Sep 30 | 1087.0 | S15N35 | $J/H/K'$ | HR 8916 |
| R Aqr | 1997 Oct 17 | 739.0 | S15N15 | $J/H/K'$ | HR 8980 |

Notes.—The baseline designations are as follows: S$x$N$y$ refers to the south telescope being at the $x$ meter station and the north telescope at the $y$ meter station. The (length, azimuth) values of the S15N15 and S15N35 baselines are (21 m, $-3\overset{\circ}{.}8$) and (38 m, $+18^\circ$), respectively.

and Millan-Gabet et al. (2001). For each interferogram, a peak fringe visibility (the fringe amplitude relative to the mean flux detected) is estimated by (1) correcting the intrinsic detector nonlinearity, (2) sky subtraction, (3) subtracting the normalized outputs of the beam splitter to enhance the signal-to-noise ratio, and (4) fitting the central three fringes of the resulting interferograms in the time domain to a point source response template computed as the Fourier transform of the spectral bandpass used in the observation.

As a result of the fringe-fitting procedure, we obtain the following quantities for each interferogram: mean, fringe amplitude, position of the central fringe, and sampling rate. The data are flagged as being a false fringe identification if an individual fringe visibility is outside the range 0.0–1.0 or if either the central fringe position or sampling rate has a value that is more than 3 times the standard deviation obtained from the ensemble of the 500 reduced interferograms in the observation. Finally, an entire observation is rejected if the standard deviation of the central fringe position values exceeds $L/2$, where $L = 120$ $\mu$m is the OPD sweep for each interferogram.

For each observation, the above procedure results in several hundred estimates of the fringe visibility: one per interferogram that survives the flagging procedure. A final estimate for the observation is formed as the mean of those values, with an internal statistical error given by the error in the mean.

Calibrator stars are measured close in space and time to the target observations in order to estimate the instrument's system visibility. Calibrated visibility amplitudes are obtained by dividing the target visibilities by estimates of the system visibility at the time of the target observations formed by spline interpolation of the calibrator observations. A correction to the system visibility resulting from the finite but known size of the calibrator stars is applied. Standard error propagation is used to include in the calibrated visibility the error resulting from the division by the system visibility and the systematic error resulting from the uncertainty in the calibrator star sizes.

The calibrator sizes and uncertainties are listed in Table 3; these values were estimated as follows: (1) if available, adopt a near-infrared direct measurement from the CHARM catalog (Richichi & Percheron 2002); or else (2) if available, adopt the value based on stellar atmosphere modeling of Borde et al. (2002) or Cohen et al. (1999); or else (3) if available, and if the star is a luminosity class I, II, or III, use the empirical size-color relations of van Belle (1999); or else (4) fit the available visual

TABLE 3
CALIBRATOR ESTIMATED DIAMETERS AND UNCERTAINTIES

| CALIBRATOR | | | ANGULAR DIAMETER | |
|---|---|---|---|---|
| HR Number | HD Number | SPECTRAL TYPE | (mas) | REFERENCE |
| HR 82 | HD 1671 | F5 III | 0.65 ± 0.08 | 1a |
| HR 175 | HD 3817 | G8 III | 1.19 ± 0.15 | 3 |
| HR 353 | HD 7147 | K4 III | 1.59 ± 0.20 | 3 |
| HR 470 | HD 10110 | K5 III | 1.84 ± 0.02 | 2 |
| HR 787 | HD 16735 | K0 II | 1.29 ± 0.16 | 3 |
| HR 876 | HD 18339 | K3 III | 1.45 ± 0.18 | 3 |
| HR 978 | HD 20277 | G8 IV | 1.14 ± 0.09 | 4 |
| HR 1133 | HD 23193 | A2m | 0.23 ± 0.04 | 4 |
| HR 1588 | HD 31579 | K4 III | 1.78 ± 0.23 | 3 |
| HR 1698 | HD 33856 | K3 III | 2.13 ± 0.02 | 1b |
| HR 1830 | HD 36134 | K1 III | 1.29 ± 0.16 | 3 |
| HR 1866 | HD 36678 | M0 III | 2.55 ± 0.03 | 2 |
| HR 2047 | HD 39587 | G0 V | 1.11 ± 0.20 | 4 |
| HR 2105 | HD 40486 | K0 | 1.87 ± 1.33 | 4 |
| HR 2169 | HD 42049 | K4 III | 2.17 ± 0.28 | 3 |
| HR 2188 | HD 42466 | K1 III | 0.96 ± 0.12 | 3 |
| HR 2338 | HD 45466 | K4 III | 2.17 ± 0.28 | 3 |
| HR 2864 | HD 59294 | K1 III | 2.24 ± 0.03 | 2 |
| HR 3115 | HD 65522 | K2 | 1.50 ± 0.98 | 4 |
| HR 3319 | HD 71250 | M3 III | 4.61 ± 0.60 | 3 |
| HR 3791 | HD 82522 | K4 III | 1.13 ± 0.14 | 3 |
| HR 3877 | HD 84561 | K4 III | 2.15 ± 0.27 | 3 |
| HR 4081 | HD 90040 | K1 III | 1.48 ± 0.19 | 3 |
| HR 4958 | HD 114149 | K0 III | 1.51 ± 0.19 | 3 |
| HR 5020 | HD 115659 | G8 III | 3.27 ± 0.41 | 3 |
| HR 5228 | HD 121156 | K2 III | 0.96 ± 0.12 | 3 |
| HR 5312 | HD 124206 | K3 III | 1.78 ± 0.22 | 3 |
| HR 5674 | HD 135438 | K5 | 2.57 ± 2.70 | 4 |
| HR 5824 | HD 139663 | K3 III | 1.99 ± 0.02 | 2 |
| HR 5940 | HD 142980 | K1 IV | 1.27 ± 0.16 | 3 |
| HR 6065 | HD 146388 | K3 III | 1.22 ± 0.15 | 3 |
| HR 6542 | HD 159353 | K0 III | 1.10 ± 0.14 | 3 |
| HR 6770 | HD 165760 | G8 III | 1.74 ± 0.22 | 3 |
| HR 6793 | HD 166229 | K2 III | 1.56 ± 0.20 | 3 |
| HR 7192 | HD 176670 | K3 III | 2.33 ± 0.03 | 2 |
| HR 7557 | HD 187642 | A7 V | 3.25 ± 0.41 | 1c |
| HR 7804 | HD 194258 | M5 III | 6.62 ± 0.87 | 3 |
| HR 8608 | HD 214298 | K5 | 1.77 ± 0.87 | 4 |
| HR 8916 | HD 220954 | K1 III | 1.94 ± 0.02 | 2 |
| HR 8961 | HD 222107 | G8 III | 2.64 ± 0.33 | 3 |
| HR 8980 | HD 222547 | K4 III | 2.73 ± 0.35 | 3 |
| HR 8987 | HD 222643 | K3 III | 2.00 ± 0.25 | 3 |
| HR 9010 | HD 223173 | K3 II | 2.48 ± 0.32 | 3 |
| HR 9029 | HD 223559 | K4 III | 2.15 ± 0.27 | 3 |
| HR 9051 | HD 224128 | K5 | 1.49 ± 0.55 | 4 |

REFERENCES.—(1) From CHARM catalog (Richichi & Percheron 2002); (1a) Lane et al. 2001; (1b) Cohen et al. 1999; (1c) van Belle et al. 2001; (2) Borde et al. 2002; (3) van Belle 1999; (4) *getCal*/*Fbol*.

and infrared photometry with a stellar blackbody model using the *Fbol* module of the *getCal* software.[7]

In order to obtain characteristic sizes at each wavelength, the calibrated visibility data obtained at each spectral band were fitted using a simple uniform disk (UD) model for the stellar brightness. Although it is well known that for Mira stars the UD is in most cases not a good representation of the true center-to-limb variation (CLV), reconstruction of the true CLV is not possible when only sparsely sampled visibility data are available. In near-continuum bandpasses, however, where near-infrared filters are to a large extent, UD profiles are expected to approximate the CLV better than at other wavelengths (Scholz 2003). Moreover, all the visibility data presented here were obtained at spatial frequencies well inside the first lobe of the visibility function (except for one star, R Leo, as discussed in § 4), where departures from the UD intensity profile are virtually undistinguishable, and therefore baseline-dependent errors are expected to be minimal in this data set.

In Figure 1, we show four representative examples (out of a total of 34 similar observations) of the data and fitting results. The examples are chosen to illustrate distinct aspects of the data. The top two panels illustrate the general trend found that

[7] *getCal* is a software package for planning of interferometer observations produced by the Michelson Science Center at the California Institute of Technology (http://msc.caltech.edu/software/index.html).

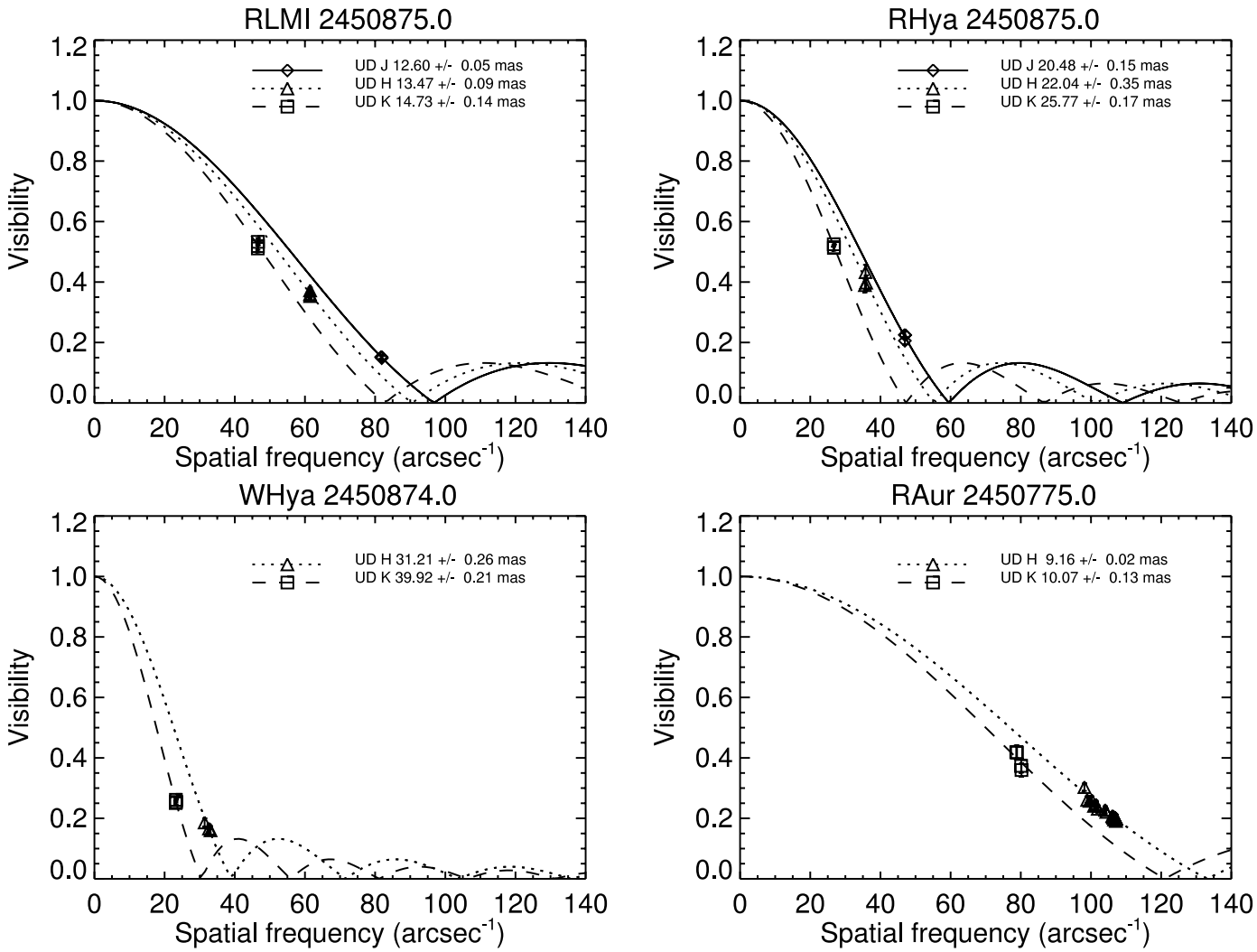


FIG. 1.—Examples of visibility data. The four panels illustrate the general finding that lower visibilities are measured at the longer near-infrared wavelengths ($J$ diameter $<$ $H$ diameter $<$ $K'$ diameter). The bottom right panel also illustrates the data precision. In all panels the abscissa is the spatial frequency given by the projected baseline $B_p/\lambda_0 = (u^2 + v^2)^{1/2}$, and the ordinate is the visibility amplitude (1.0 for a pointlike source and 0.0 for a completely resolved extended source).

$J$ diameter $<$ $H$ diameter $<$ $K'$ diameter. The bottom left panel illustrates our ability to sample relatively low visibilities for bright sources. The bottom right panel shows an example in which Earth rotation allowed sampling of a relatively large range of projected baseline length, illustrating the visibility data precision for observations within a single night; here the visibility fit rms is 0.01, or 3.8% of the (changing) model visibility, which is a typical value for the data set (full range is 1%–10%).

The night-to-night data consistency was evaluated by comparing the results obtained when the same star was observed on different nights, at a similar pulsational phase and using the same baseline, in order to isolate the test from possible size variations and noncircular star shapes. There are three such cases in our data set (times three bands for a total of nine independent comparisons), and the result is that the night-to-night consistency in visibility is in all cases better than 8%, with mean values of 2.3%, 3.0%, and 3.8% for the $J$, $H$, and $K'$ bands, respectively.

Our data can also be compared with previous measurements from the literature. This comparison can only be made at the $K$ band. Considering the most recent measurements (Perrin et al. 1999; van Belle et al. 2002; Monnier et al. 2004), we find that (1) our diameters show no systematic positive or negative bias with respect to the literature values and (2) the diameter values agree to 20% or better. Considering that no effort was made to compare data taken only at similar pulsational phases, this level of agreement appears reasonable, given, for example, that $K$-band Mira sizes can change by 10% for a phase difference of only 0.04 (Perrin et al. 1999).

## 4. RESULTS

Recognizing that potentially the best use of our $JHK'$ measurements will be as part of a larger modeling effort that incorporates for each star all the available data across the spectrum, a goal beyond the scope of this paper, we provide in Table 4 the totality of our visibility measurements. Columns (1)–(4) give the star name, calendar and Julian observation epoch, and filters used. Columns (5)–(7) give the two-dimensional spatial frequencies ($u$, $v$) and measured visibilities.

In addition, in order to capture the essential features of the size-wavelength relation across the near-infrared, we provide in Table 5 the results of fitting our visibility data to UD models. Columns (1)–(4) give the star name, the observation Julian

TABLE 4

CALIBRATED VISIBILITY DATA

| Name (1) | Date (2) | Julian Date (3) | Filter (4) | $u$ (arcsec$^{-1}$) (5) | $v$ (arcsec$^{-1}$) (6) | Visibility Amplitude (7) |
|---|---|---|---|---|---|---|
| R And..... | 1997 Nov 21 | 2,450,774 | $H$ | −2.22 | 112.25 | 0.463 ± 0.035 |
| R And..... | 1997 Nov 21 | 2,450,774 | $H$ | −4.79 | 112.16 | 0.419 ± 0.035 |
| R And..... | 1997 Nov 21 | 2,450,774 | $H$ | −12.91 | 111.48 | 0.485 ± 0.035 |
| R And..... | 1997 Nov 21 | 2,450,774 | $K'$ | −13.46 | 83.05 | 0.766 ± 0.040 |
| R And..... | 1997 Nov 21 | 2,450,774 | $K'$ | −15.92 | 82.57 | 0.712 ± 0.040 |
| Z Cet ..... | 1998 Nov 4 | 2,451,122 | $J$ | 57.79 | 118.31 | 0.858 ± 0.026 |
| Z Cet ..... | 1998 Nov 4 | 2,451,122 | $J$ | 54.73 | 118.25 | 0.850 ± 0.026 |
| Z Cet ..... | 1998 Nov 4 | 2,451,122 | $J$ | 51.98 | 118.19 | 0.863 ± 0.026 |
| Z Cet ..... | 1998 Nov 4 | 2,451,122 | $H$ | 52.04 | 89.86 | 0.858 ± 0.021 |
| Z Cet ..... | 1998 Nov 4 | 2,451,122 | $H$ | 50.23 | 89.80 | 0.843 ± 0.021 |
| Z Cet ..... | 1998 Nov 4 | 2,451,122 | $H$ | 48.24 | 89.74 | 0.838 ± 0.021 |
| Z Cet ..... | 1998 Nov 4 | 2,451,122 | $K'$ | 26.08 | 67.09 | 0.913 ± 0.010 |
| Z Cet ..... | 1998 Nov 4 | 2,451,122 | $K'$ | 24.98 | 67.07 | 0.918 ± 0.010 |
| U Per..... | 1997 Nov 19 | 2,450,772 | $J$ | −10.34 | 140.05 | 0.509 ± 0.022 |
| U Per..... | 1997 Nov 19 | 2,450,772 | $J$ | −14.74 | 139.53 | 0.515 ± 0.022 |

NOTE.—Table 4 is published in its entirety in the electronic edition of the *Astrophysical Journal*. A portion is shown here for guidance regarding its form and content.

TABLE 5

NEAR-INFRARED ANGULAR DIAMETERS AND DIAMETER RATIOS

| Name (1) | Julian Date (−2,450,000) (2) | Phase (3) | Phased Spectral Type (M subclass) (4) | $D_J$ (mas) (5) | $D_H$ (mas) (6) | $D_K$ (mas) (7) | $R_{J/H}$ (8) | $R_{H/K}$ (9) |
|---|---|---|---|---|---|---|---|---|
| R And..... | 0774.0 | 0.6 | 6.0 | ... | 6.6 ± 0.2 | 5.7 ± 0.3 | ... | 1.16 ± 0.07 |
| Z Cet ..... | 1122.0 | 0.25 | 5.0 | 2.7 ± 0.2 | 3.5 ± 0.2 | 3.7 ± 0.2 | 0.76 ± 0.05 | 0.95 ± 0.06 |
| U Per..... | 0772.0 | 0.8 | 6.0 | 5.0 ± 0.1 | 5.4 ± 0.1 | 6.6 ± 0.2 | 0.93 ± 0.02 | 0.83 ± 0.03 |
| U Per..... | 1088.0 | 0.9 | 5.5 | 4.5 ± 0.1 | 4.85 ± 0.05 | 5.0 ± 0.3 | 0.93 ± 0.01 | 0.97 ± 0.05 |
| R Per ..... | 1089.0 | 0.3 | 6.3 | <1.6 | <0.9 | <2.7 | ... | ... |
| R Per ..... | 1123.0 | 0.5 | 7.5 | <1.5 | <2.2 | <1.8 | ... | ... |
| R Aur ..... | 0734.0 | 0.7 | 8.5 | 11.1 ± 0.1 | 10.5 ± 0.3 | ... | 1.05 ± 0.03 | ... |
| R Aur ..... | 0772.0 | 0.8 | 8.5 | ... | 9.3 ± 0.1 | 10.1 ± 0.1 | ... | 0.92 ± 0.01 |
| R Aur ..... | 0775.0 | 0.8 | 8.5 | ... | 9.2 ± 0.1 | 10.1 ± 0.1 | ... | 0.91 ± 0.01 |
| S Ori..... | 1123.0 | 0.1 | 6.3 | ... | 9.1 ± 0.1 | 9.6 ± 0.2 | ... | 0.95 ± 0.02 |
| U Ori..... | 0739.0 | 0.9 | 9.0 | 10.9 ± 0.1 | 12.5 ± 0.1 | ... | 0.87 ± 0.01 | ... |
| U Ori..... | 0774.0 | 0.04 | 8.2 | 11.5 ± 0.1 | ... | ... | ... | ... |
| U Ori..... | 0776.0 | 0.04 | 8.2 | ... | 9.2 ± 0.3 | 10.5 ± 0.4 | ... | 0.87 ± 0.05 |
| X Aur..... | 0736.0 | 0.1 | 3.4 | <3.3 | <3.2 | <5.2 | ... | ... |
| R Cnc..... | 0875.0 | 0.4 | 7.5 | ... | 15.3 ± 0.2 | 18.9 ± 0.2 | ... | 0.81 ± 0.01 |
| R LMi ..... | 0773.0 | 0.2 | 8.0 | ... | ... | 12.1 ± 0.1 | ... | ... |
| R LMi ..... | 0873.0 | 0.5 | 9.0 | 12.5 ± 0.1 | 12.8 ± 0.2 | 14.2 ± 0.2 | 0.97 ± 0.01 | 0.91 ± 0.02 |
| R LMi ..... | 0875.0 | 0.5 | 9.0 | 12.6 ± 0.1 | 13.5 ± 0.1 | 14.7 ± 0.1 | 0.94 ± 0.01 | 0.91 ± 0.01 |
| R Leo ..... | 0874.0 | 0.4 | 7.5 | ... | 23.8 ± 0.3 | 29.91 ± 0.27 | ... | 0.79 ± 0.01 |
| | | | | | 32.4 ± 0.4 | ... | ... | ... |
| R Hya..... | 0873.0 | 0.8 | 8.0 | 19.8 ± 1.1 | 22.7 ± 0.6 | 23.9 ± 0.5 | 0.87 ± 0.05 | 0.95 ± 0.03 |
| R Hya..... | 0875.0 | 0.8 | 8.0 | 20.5 ± 0.2 | 22.0 ± 0.4 | 25.8 ± 0.2 | 0.93 ± 0.02 | 0.86 ± 0.01 |
| W Hya..... | 0874.0 | 0.6 | 7.0 | ... | 31.2 ± 0.3 | 39.9 ± 0.2 | ... | 0.78 ± 0.01 |
| S Crb..... | 0874.0 | 0.4 | 7.5 | 9.2 ± 0.7 | 8.9 ± 0.9 | 9.2 ± 0.9 | 1.04 ± 0.13 | 0.96 ± 0.14 |
| S Crb..... | 0977.0 | 0.6 | 9.0 | ... | 9.1 ± 0.5 | 11.2 ± 0.4 | ... | 0.81 ± 0.05 |
| RS Lib..... | 0873.0 | 1.0 | 7.5 | 9.8 ± 0.4 | 9.1 ± 0.9 | 9.3 ± 1.1 | 1.08 ± 0.11 | 0.98 ± 0.15 |
| R Ser ..... | 0875.0 | 0.0 | 4.0 | 7.5 ± 0.1 | 8.3 ± 0.7 | 10.4 ± 0.4 | 0.90 ± 0.07 | 0.80 ± 0.07 |
| R Ser ..... | 0880.0 | 0.1 | 6.0 | ... | 6.8 ± 0.1 | 7.9 ± 0.1 | ... | 0.86 ± 0.01 |
| S Her..... | 0980.0 | 0.6 | 8.0 | 5.4 ± 0.3 | 5.6 ± 0.2 | ... | 0.97 ± 0.06 | ... |
| Ry Lyr..... | 0980.0 | 0.35 | 7.7 | ... | 2.7 ± 0.3 | <2.03 | ... | ... |
| R Aql..... | 0978.0 | 0.9 | 7.5 | ... | 9.3 ± 0.1 | 10.6 ± 0.1 | ... | 0.88 ± 0.01 |
| R Peg..... | 1088.0 | 0.0 | 7.0 | 6.0 ± 0.4 | 7.0 ± 0.3 | 9.6 ± 0.2 | 0.86 ± 0.06 | 0.73 ± 0.03 |
| W Peg ..... | 1088.0 | 0.1 | 6.9 | ... | 8.2 ± 0.1 | 9.6 ± 0.1 | ... | 0.86 ± 0.01 |
| S Peg..... | 1087.0 | 0.1 | 5.2 | 3.9 ± 0.1 | 4.9 ± 0.3 | 4.8 ± 0.5 | 0.79 ± 0.05 | 1.02 ± 0.12 |
| R Aqr ..... | 0739.0 | 0.4 | 7.5 | 17.7 ± 0.2 | 17.7 ± 0.1 | 20.8 ± 0.8 | 1.00 ± 0.01 | 0.85 ± 0.03 |

NOTES.—For R Leo, the two $H$-band diameter values indicated correspond to the two possible solutions that exist in the second lobe of the visibility function. See § 4 for discussion.

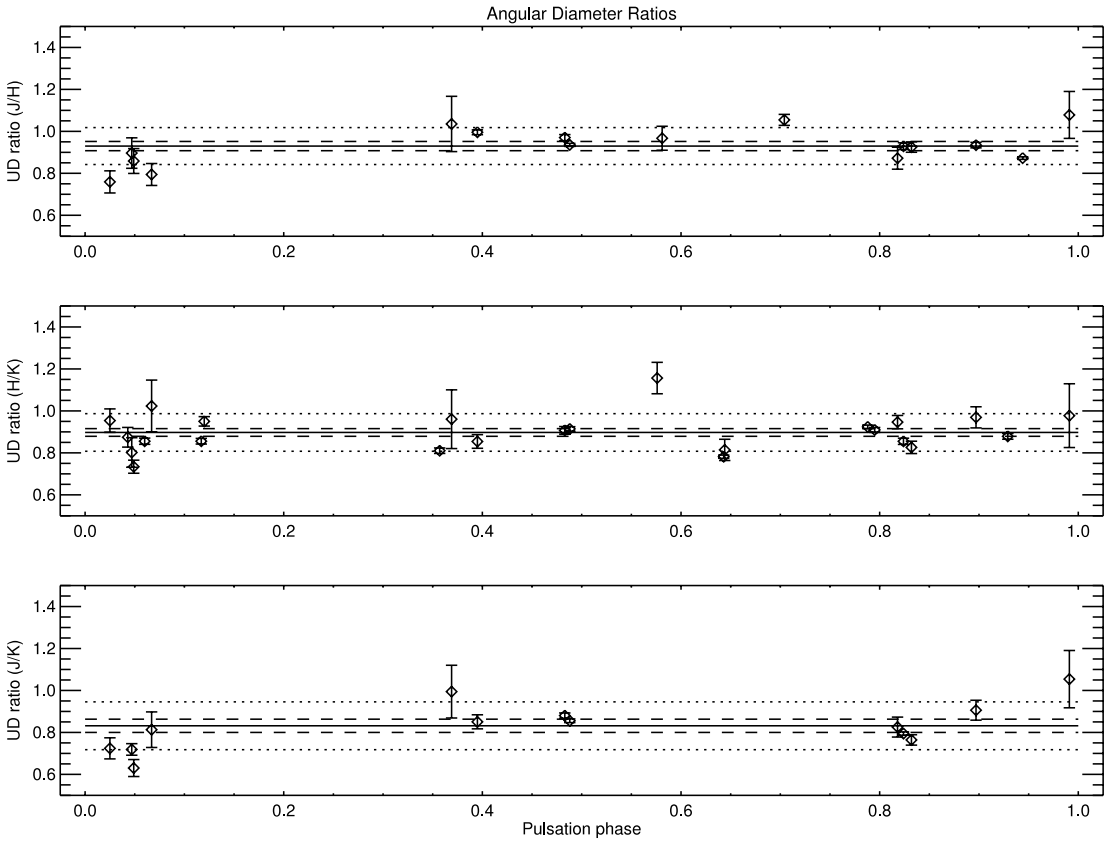


FIG. 2.—Angular diameter ratios. For each panel the solid line indicates the measured mean ratio, the dashed lines indicate the error in the mean, and the dotted lines indicate the rms of the sample.

date, the pulsation phase,[8] and an estimate of the spectral type for that pulsation phase (see § 5). Columns (5)–(7) give the *J*-, *H*-, and $K'$-band best-fit UD diameters. The fact that we have measurements at three different wavelengths allows us to make a relative measurement in terms of diameter *ratios*, given in columns (8)–(9), which are expected to be immune to some sources of systematic error (e.g., calibrator diameter uncertainty, seeing effects) and also represent the linear size ratios independent of (uncertain) distances.

For R Leo, essentially a single spatial frequency was sampled at the *H* and $K'$ bands, and the visibilities are sufficiently low that mathematically, three solutions to the UD fit exist: one in the main lobe of the visibility function and two in the second lobe. We therefore use a priori knowledge of R Leo's nominal near-infrared size to further constrain our solutions. For the $K'$ band, we use the diameter measured by Monnier et al. (2004; $30.3 \pm 0.2$ mas) as a starting value for the fit. For the *H* band, we use the unpublished value obtained by one of us (J. D. Monnier) from aperture masking at the Keck telescope ($\sim$30 mas) to obtain the two first-lobe solutions indicated in Table 5. Without spatial frequency coverage that follows the shape of the visibility function, it is not possible to discriminate between these solutions, and therefore we have dropped this star from the analysis that follows.

[8] For each observation we have estimated the pulsation phase at the observation epoch as follows. The AFOEV (http://cdsweb.u-strasbg.fr/afoev) and AAVSO (http://www.aavso.org) databases were used to obtain the epochs of maximum light before and after the IOTA observation, $o_{\max 1}$ and $o_{\max 2}$, respectively. The phase at the IOTA epoch is then estimated as phase = (IOTA epoch − $o_{\max 1}$)/($o_{\max 2} - o_{\max 1}$).

As is apparent in Table 5, the basic result of this paper is that the near-infrared diameters are found to follow the trend *J* diameter $<$ *H* diameter $<$ $K'$ diameter. This result is also illustrated in Figure 2, where the angular diameter ratios are plotted as a function of pulsation phase. The mean values of the diameter ratios are

$$\overline{R_{J/H}} = 0.93 \pm 0.02,$$
$$\overline{R_{H/K'}} = 0.89 \pm 0.02,$$

where the 1 $\sigma$ uncertainty is given by the error in the mean and the (sample rms, number of observations) values are (0.09, 16) and (0.09, 24) for *J*/*H* and *H*/$K'$, respectively.

We finally comment on a few cases for which there are intriguing changes in the measured sizes, above the levels of calibration accuracy demonstrated in § 3. As can be seen in Table 5, whenever there is both a significant time difference between two epochs of observation and a difference in the baselines used, apparent size changes in the range 10%–30% can occur (R Aur, U Ori, R LMi, S CrB, and R Ser). Given the variety of possible effects at play, however (physical changes in the stars, inadequacy of the UD model, stellar asymmetries probed for different baseline orientations), it is difficult to assess whether these effects are real or arise from unusually high calibration errors. These issues might be resolved with further observations.

## 5. DISCUSSION

We have measured the diameters of 23 Mira stars simultaneously in the near-continuum near-infrared *J*, *H*, and $K'$ bands,

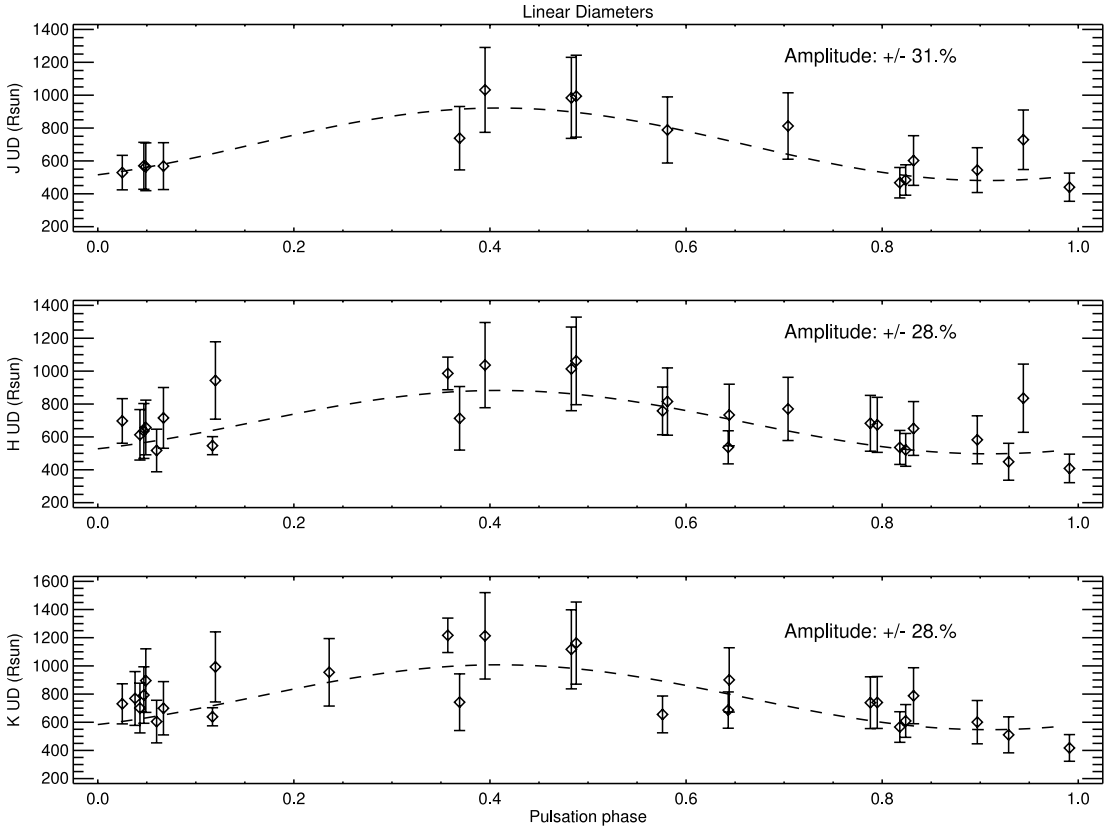


FIG. 3.—Linear diameters as a function of pulsation phase. In each panel the dashed line indicates a sinusoidal fit to the data. The sinusoidal fits have four free parameters, mean, amplitude, period, and phase, except for the $K'$-band data, where we fix the period and phase to the values found in the $J$ and $H$ fits. See § 5 for discussion.

a first for each star in the sample. The simultaneity of the measurements guarantees that the same physical state of the star is measured in each band. We find the apparent size relation $J$ diameter $<$ $H$ diameter $<$ $K'$ diameter, in agreement with expectations that the shorter near-infrared filter ($J$ band) better samples the true photospheric continuum and that the $H$ and $K'$ filters contain progressively more opacity contamination from molecules in higher layers (see, e.g., Jacob & Scholz 2002). In terms of the magnitude of the size difference, or diameter ratios, we find that the stars appear to be as much as 24% smaller at $J$ than at the $H$ band (mean 8%) and as much as 27% smaller at $H$ than at the $K'$ band (mean 11%). These magnitudes are in general agreement with the models of Jacob & Scholz (2002) and Ireland et al. (2004a), although clearly detailed comparisons must be made for specific stars and specific models.

Changes in the near-infrared sizes of individual Mira stars as a function of pulsation phase have been detected interferometrically (Perrin et al. 1999; Thompson 2002; Thompson et al. 2002). No single star in our sample has sufficient phase coverage for such a study. However, we have attempted to detect the pulsation by treating the sample as a single "synthetic" Mira. A priori, the most promising approach appeared to be to explore this effect using the size ratios, because of their calibration advantages. However, as is apparent in Figure 2, no sinusoidal signature is present. We have also explored the possibility that the pulsation was not seen in the above approach because of the fact that instantaneous spectral type, rather than pulsation phase, might be the relevant parameter. Thus, we have used "phased spectral types" (col. [4] of Table 5) from the literature (Terrill 1969; Lockwood & Wing 1971; Lockwood 1972) to search for a monotonic relation (also for the synthetic Mira) between the measured apparent sizes and the spectral type measured for the corresponding pulsation phase, also without success.

Forsaking the advantages of distance independence, then, we show in Figure 3 our measured $J$, $H$, and $K'$ linear sizes as a function of pulsation phase. As discussed by van Belle et al. (2002), *Hipparcos* distances to Mira stars are rather uncertain, and therefore we have used distances from the literature based on period-luminosity (PL) relations, as indicated in Table 1. We note that we do not attempt to apply the PL relations using estimates of the absolute $K$-band magnitudes based on our own fringe data, because the instrumentation and observing strategy were never intended for accurate photometry. Although the data errors are relatively large and systematic deviations are apparent, the data suggest a sinusoidal signature with maximum sizes near phase = 0.5 (minimum light), as expected (as the photospheric size increases and cools, the star becomes fainter). The statistical significance of the sinusoidal signature is, however, marginal, with reduced $\chi^2$ of 0.4, 0.8, and 0.9 at $J$, $H$, and $K'$ bands, respectively, compared with 1.9, 2.0, and 2.2 for models consisting of the constant average diameters. We note that while the observed sinusoid amplitudes (50%–60% peak-to-peak) are comparable to those obtained from model predictions (Ireland et al. 2004a), they are considerably larger than observed (9%–26% peak-to-peak) when individual Mira stars are followed through their pulsation cycles (Thompson 2002; Thompson et al. 2002). In addition, it can be seen in Figure 3 that the linear sizes vary rather in unison, explaining why the pulsation was not apparent in the diameter ratios of Figure 2.

Ultimately, we believe that the failure to more convincingly detect the pulsation using the approaches just described is due

to the fundamental inadequacy of those methods, as several physical mechanisms may contribute dispersion at levels comparable to the expected signatures: (1) there are intrinsic star-to-star differences; (2) our filters are broadband and therefore probe a complex combination of emission from multiple layers of molecular gas just above the photosphere, with opacities that also change during the pulsation, making the true expected signature very complicated and in particular potentially masking the photospheric layer motions (Ireland et al. 2004a); and (3) some theoretical models predict cycle-to-cycle nonrepeatability of the photospheric diameters at significant levels (tens of percent; Jacob & Scholz 2002; Ireland et al. 2004a), which, if present, would introduce that much dispersion in our apparent size versus phase relations. On the last point, we note, however, that for the only published multicycle measurements to date (Thompson 2002; Thompson et al. 2002) this effect was not observed, although it appears to be present (at 5%–15% levels) in yet unpublished data by the same group (R. R. Thompson 2004, private communication). In the literature, the success of the synthetic Mira method is mixed: while van Belle et al. (1996) saw a 20% peak-to-peak change in the effective temperatures of a sample of 18 Mira stars, the effect was not explored in the 22 star sample of their follow-up paper (van Belle et al. 2002) and appears not to be present by straightforward plotting of their published numbers. We finally note that the best case in our sample in which to search for a pulsation signature of an individual star (U Per, period = 320 days) was observed at two epochs almost exactly one cycle apart, and the measured UD sizes differ by 10%, 12%, and 6% at $J$, $H$, and $K'$ bands, respectively, a marginally significant size change.

Several optical interferometers around the world are now equipped to measure accurate visibilities in broad or narrow spectral bands and together span the visible to mid-infrared spectrum. Although recent efforts over more limited regions of the spectrum have clearly illustrated the power of multiwavelength spatially resolved observations (Perrin et al. 2004; Jacob et al. 2004; Ohnaka 2004; Weiner 2004), global modeling has not been attempted to date, but represents the necessary next step toward a better theoretical understanding of Mira star atmospheres and dynamics.

The authors wish to acknowledge fruitful discussions with Robert Thompson, Gerard van Belle, and Sam Ragland. This work has made use of services produced by the Michelson Science Center at the California Institute of Technology. This research has made use of the SIMBAD database, operated at CDS, Strasbourg, France. This research has made use of the NASA/IPAC Infrared Science Archive, which is operated by the Jet Propulsion Laboratory, California Institute of Technology, under contract with the National Aeronautics and Space Administration. This research has made use of NASA's Astrophysics Data System Service. E. P. wishes to acknowledge that part of this work was performed while he was a predoctoral fellow of the Smithsonian Astrophysical Observatory.

REFERENCES

Bonneau, D., Foy, R., Blazit, A., & Labeyrie, A. 1982, A&A, 106, 235
Bonneau, D., & Labeyrie, A. 1973, ApJ, 181, L1
Borde, P., Coude du Foresto, V., Chagnon, G., & Perrin, G. 2002, A&A, 393, 183
Cohen, M., Walker, R. G., Carter, B., Hammersley, P., Kidger, M., & Noguchi, K. 1999, AJ, 117, 1864
Haniff, C. A., Scholz, M., & Tuthill, P. G. 1995, MNRAS, 276, 640
Hofmann, K.-H., et al. 2000, A&A, 353, 1016
———. 2001, A&A, 376, 518
———. 2002, NewA, 7, 9
Ireland, M. J., Scholz, M., & Wood, P. R. 2004a, MNRAS, 352, 318
Ireland, M. J., Tuthill, P. G., Bedding, T. R., Robertson, J. G., & Jacob, A. P. 2004b, MNRAS, 350, 365
Jacob, A. P., Bedding, T. R., Robertson, J. G., Barton, J. R., Haniff, C. A., & Marson, R. G. 2004, MNRAS, 349, 303
Jacob, A. P., & Scholz, M. 2002, MNRAS, 336, 1377
Jura, M., & Kleinmann, S. G. 1992, ApJS, 79, 105
Labeyrie, A., Koechlin, L., Bonneau, D., Blazit, A., & Foy, R. 1977, ApJ, 218, L75
Lane, B. F., Boden, A. F., & Kulkarni, S. R. 2001, ApJ, 551, L81
Lockwood, G. W. 1972, ApJS, 24, 375
Lockwood, G. W., & Wing, R. F. 1971, ApJ, 169, 63
Mennesson, B., et al. 2002, ApJ, 579, 446
Millan-Gabet, R. 1999, Ph.D. thesis, Univ. Massachusetts (Amherst)
Millan-Gabet, R., Schloerb, F. P., & Traub, W. A. 2001, ApJ, 546, 358
Millan-Gabet, R., Schloerb, F. P., Traub, W. A., & Carleton, N. P. 1999, PASP, 111, 238
Monnier, J. D., et al. 2004, ApJ, 605, 436
Ohnaka, K. 2004, A&A, 421, 1149
Perrin, G., et al. 1999, A&A, 345, 221
———. 2004, A&A, 426, 279
Richichi, A., & Percheron, I. 2002, A&A, 386, 492
Scholz, M. 2003, Proc. SPIE, 4838, 163
Terrill, C. L. 1969, AJ, 74, 413
Thompson, R. R. 2002, Ph.D. thesis, Univ. Wyoming
Thompson, R. R., Creech-Eakman, M. J., & van Belle, G. T. 2002, ApJ, 577, 447
Traub, W. A. 1998, Proc. SPIE, 3350, 848
Tuthill, P. G., Danchi, W. C., Hale, D. S., Monnier, J. D., & Townes, C. H. 2000a, ApJ, 534, 907
Tuthill, P. G., Haniff, C. A., Baldwin, J. E., & Feast, M. W. 1994, MNRAS, 266, 745
Tuthill, P. G., Monnier, J. D., & Danchi, W. C. 2000b, Proc. SPIE, 4006, 491
van Belle, G. T. 1999, PASP, 111, 1515
van Belle, G. T., Ciardi, D. R., Thompson, R. R., Akeson, R. L., & Lada, E. A. 2001, ApJ, 559, 1155
van Belle, G. T., Dyck, H. M., Benson, J. A., & Lacasse, M. G. 1996, AJ, 112, 2147
van Belle, G. T., Thompson, R. R., & Creech-Eakman, M. J. 2002, AJ, 124, 1706
van Belle, G. T., et al. 1997, AJ, 114, 2150
Weigelt, G., et al. 2003, Proc. SPIE, 4838, 181
Weiner, J. 2004, ApJ, 611, L37
Weiner, J., Hale, D. D. S., & Townes, C. H. 2003a, ApJ, 588, 1064
———. 2003b, ApJ, 589, 976
Wyatt, S. P., & Cahn, J. H. 1983, ApJ, 275, 225
Young, K. 1995, ApJ, 445, 872